Observing the Non-Optically Active: An Observability Budget for Inferring Stormwater BMP Nitrogen-Removal Performance from Earth Observation

Saurav Kumar, Ph.D., F.EWRI, M.ASCE[1]

[1]Assistant Professor, School of Sustainable Engineering and the Built Environment, Arizona State University, 777 E. University Dr., Tempe, AZ 85281 (corresponding author). ORCID: https://orcid.org/0000-0002-9664-1667. Email: sk2@asu.edu

Abstract

Some regulatory load-accounting programs credit distributed stormwater best management practices (BMPs) using standardized, type-based nitrogen-removal efficiencies, yet field records show highly variable removal with at most a weak age signal. Earth observation (EO) can map aspects of a practice's physical condition, such as open-water extent and vegetation, and may provide indirect storage-related proxies, but it cannot directly observe the pollutant removal that regulation credits. This paper asks whether assimilating observed condition through a process model may recover otherwise unobservable performance, and it advances a single principle. On a proper, held-out score, assimilating remotely observed condition appears to recover treatment performance according to how much of that performance is routed through observable condition, and little beyond it. The principle is examined with a calibrated observing-system simulation experiment in which a known synthetic truth is observed with noise and reconstructed. On disjoint held-out seeds, the observability-budget skill, defined as the CRPS skill gain, the fraction of the gap to a perfect-performance reference that assimilation closes, rises with the observable share of hidden-rate-driven performance. It is only about 16% when the rate modifier is fully hidden. It reaches about 65 to 76% where the rate modifier is fully explained by observed condition, although those fully observable cells are overconfident under the known-forcing idealization and are read as an upper bound. Storage-routed aging performance is separately recovered from about 24% to 68%, because storage is observed. Because these are properties of the simulated system under stated assumptions, they are intended to bound rather than measure the operational budget, positioning the observability budget as a design quantity that targeted monitoring investment could enlarge.

Keywords: Best management practices; treatment wetlands; nitrogen removal; data assimilation; Earth observation; observability; predictive maintenance; stormwater monitoring.

Practical Applications

Agencies increasingly hope to check nitrogen removal at their many stormwater ponds and wetlands from satellite imagery, since sampling each with field crews is impractical. A satellite sees a pond's condition, not its nitrogen removal, and feeding condition into a process model may recover removal only where observable condition governs the removal rate, so elsewhere field measurement would remain necessary. This paper offers a way to quantify, for a given asset class, how much of performance might be recoverable from EO under stated assumptions, and suggests that the recoverable fraction is set by an observability budget whose operationally recoverable share targeted calibration could enlarge. In a simulated demonstration, it also points to a potentially usable result, that EO-tracked condition could support preemptive, condition-based maintenance that helps keep ponds below the maintenance threshold and protect removal, and appears to match a perfect-state threshold rule within the tested policy class while spending a comparable number of interventions. Realizing this in practice would require validation before operational use, including validated EO condition products and field testing.

Introduction

Some watershed load-accounting and nutrient-credit programs assign standardized pollutant-removal efficiencies by BMP category, including wet ponds and wetlands (Commonwealth of Virginia 2024; U.S. Environmental Protection Agency and Chesapeake Bay Program 2003). Here distributed BMPs are scoped to pond- and wetland-type stormwater BMPs (wet stormwater control measures), and extension to other BMP types (infiltration basins, bioretention, permeable pavement, hydrodynamic separators) is a hypothesis rather than a demonstrated result. Category-level values are useful for accounting, but they should not be interpreted as time-invariant, asset-specific performance. Percent removal depends on influent concentration and on the selected performance metric, and treatment response also varies with runoff volume and site and event conditions (Barrett 2005; Gilliom et al. 2020; Hoss et al. 2016; Lenhart and Hunt 2011; U.S. Environmental Protection Agency 2026). Available field records likewise show highly variable nitrogen removal: one synthesis found a weak decline in ammonium removal with BMP age but insufficient age information for nitrate and total nitrogen (Koch et al. 2014), and a recent two-pond study found that wet-pond removal varied with meteorological, hydrologic, and hydraulic conditions (Yang et al. 2023). Sediment accumulation can reduce storage and alter long-term pond function (Ahilan et al. 2019; Drake and Guo 2008), sediment properties influence nitrogen cycling within wet ponds (Gold et al. 2017), and heterogeneous vegetation can alter routing and contaminant removal (Min and Wise 2009; Sabokrouhiyeh et al. 2020). Maintenance is therefore necessary to sustain treatment function, particularly where sediment and debris accumulate (Erickson et al. 2010, 2018). In a phosphorus analog, nearly 40% of 98 Minnesota stormwater ponds had median summer total-phosphorus concentrations above typical runoff, consistent with internal phosphorus loading (Taguchi et al. 2020). A general BMP lifecycle-modeling framework represents efficiency as changing between maintenance events, declining with aging processes such as sediment accumulation or clogging, and improving after maintenance; its demonstrations concern total-phosphorus reduction by bioretention and grass buffer strips rather than nitrogen removal by ponds or wetlands (Liu et al. 2018). Motivated by that general framework, we idealize the condition and performance trajectory as a saw-tooth pattern between maintenance events: it declines as storage fills and short-circuiting develops, then partially recovers after each maintenance action, so a single credited efficiency stands in for a quantity that drifts continuously between interventions.

Repeated in situ monitoring does not readily scale across a large, distributed BMP population. EO is the measurement approach most likely to provide consistent population-scale coverage, and a recent preprint argues that, in many settings, public imagery can support extraction of per-asset footprints, types, and condition departures, with the binding constraint arguably shifting toward community benchmark data rather than satellite data (Kumar 2026). EO can map aspects of *condition*, including surface-water extent (Huang et al. 2018; Pekel et al. 2016) and vegetation greenness (Tucker 1979), but hydraulic storage loss would have to be inferred indirectly. Throughout, EO is treated as an idealized storage-related condition proxy at monthly resolution that represents an upper-bound observing system. A validated monthly retrieval of hydraulic storage loss at the assumed error level is not yet established, and the analysis assumes regular observations without cloud gaps, mixed pixels, registration error, or persistent bias. EO also does not directly measure *performance*, the in-water removal efficiency used in load accounting. The line between observable condition and unobservable performance is an observability frontier, and the central question is where, and how far, assimilation can move it.

The question of how much of this drifting performance a condition-only sensor can recover is well suited to an observing-system simulation experiment (OSSE), or twin experiment. In an OSSE, a known synthetic truth is generated from a process model, sampled through a simulated observing system with realistic noise, and then assimilated; because the truth is known by construction, the information the observing system recovers can be measured directly rather than inferred from scarce field records. The design originated in numerical weather prediction, where OSSEs have long been used to evaluate proposed observing systems before they are built (Arnold and Dey 1986), and the same reasoning now underpins data assimilation across the Earth sciences (Evensen 2003; Reichle 2008). Applied to distributed BMPs, an OSSE makes it possible to ask, before committing monitoring resources, how much treatment performance a satellite that sees only condition can recover through a process model, and where that recovery reaches its limit.

Against this background, the study pursues three connected aims. The first aim is conceptual. It defines the observability budget as the fraction of the attainable probabilistic improvement in performance inference that assimilating observable condition recovers, for a specified sensor suite, process model, and prior, so the complement is a largely irreducible gap under those same assumptions rather than a fundamental limit on what any instrument could measure. The second aim is quantitative. It explores that observability budget with a calibrated OSSE and suggests that recovery is partial and appears to be governed by the degree to which observable condition is assigned control of the removal rate in the simulation, a pattern that seems to persist across process structures and aging mechanisms. The third aim is practical. It asks whether, although performance itself is only partially recoverable, condition might be recovered well enough to support condition-based maintenance that helps protect the performance the sensor never measures.

Two questions organize the study. First, for a given asset class, how much of drifting treatment performance can a condition-only observing system recover, and what sets that share? Second, even where performance itself is only partially recoverable, can observed condition be recovered well enough to support condition-based maintenance that helps protect the performance the sensor never measures? Developed here for nitrogen, the framework may extend to other pollutants whose removal is condition-governed, which we offer as a hypothesis rather than a demonstrated result.

Methods

The overall approach is summarized in Fig. 1, and the complete experimental design is laid out in the Supplementary Material (Fig. S1). EO supplies noisy observations of BMP condition, which are assimilated with an ensemble Kalman filter, an ensemble method that updates model states from noisy observations while tracking their uncertainty, into a condition-dependent process model to infer the unobservable nitrogen-removal performance; a hidden biogeochemical forcing governs the removal rate but is never observed.

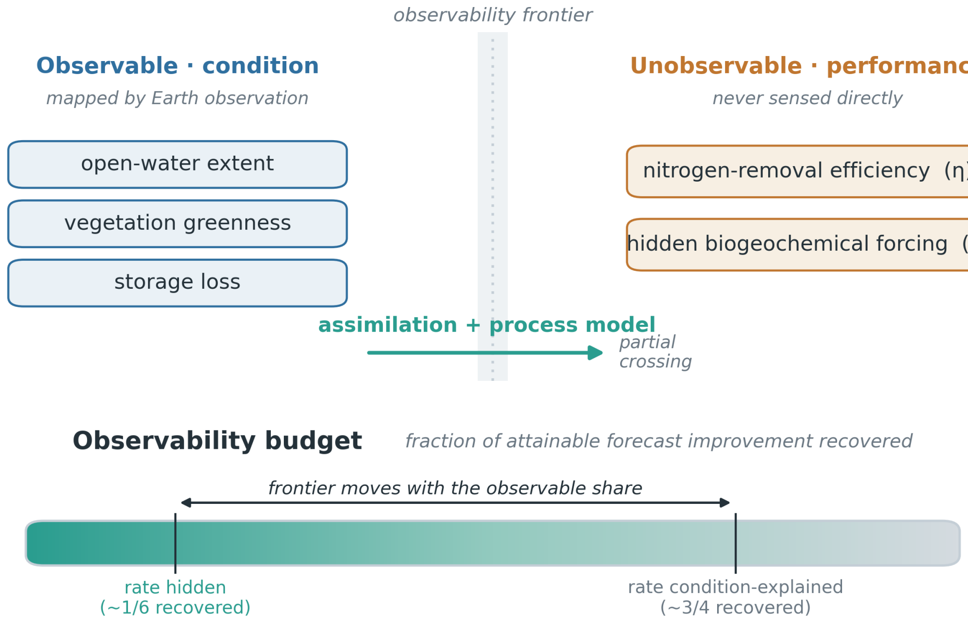

Fig. 1. Method overview and the observability frontier. EO measures a practice's *condition* (open-water extent, vegetation greenness, storage loss), which lies on the observable side of an observability frontier; treatment *performance* (nitrogen-removal efficiency η) lies on the unobservable side, together with the hidden biogeochemical forcing c that co-determines it and is never observed. A condition-dependent process model with ensemble Kalman assimilation infers performance from condition, crossing the frontier only partially. The recovered fraction of attainable probabilistic forecast improvement is the observability budget, and the remainder is largely irreducible within the stated observing system, set by the hidden forcing (bottom bar). Supplementary Fig. S1 details the full experimental design.

Inference problem

A simple wetland or vegetative BMP is described at a monthly step t by a state $\mathbf{x}_t = [s_t, v_t, \ln k_t]$, comprising the sediment-induced storage-loss fraction s, the dimensionless fractional loss of design hydraulic storage capacity due to sediment filling ($s = 0$ no loss, $s = 1$ complete loss, remaining capacity $1 - s$); the vegetation density v, a normalized vegetation-condition state whose observation operator assumes a calibrated one-to-one mapping to a normalized EO vegetation index that in practice would need a site- or asset-class-specific retrieval; and a first-order areal removal-rate k. A hidden biogeochemical forcing c_t, a dimensionless composite biogeochemical rate multiplier representing unresolved rate controls (electron-donor supply, redox, nitrate speciation, microbial state, none remotely sensed), modulates the rate, and its linear decline over the record is a stress scenario rather than a mechanistic carbon, redox, or microbial model; flow Q_t and temperature T_t are exogenous. Performance is the nitrate-nitrogen removal efficiency η_t, never observed. Here η is a fractional concentration-removal efficiency, a normalized treatment-efficiency proxy, not load-weighted mass removed. Observations map condition only, $\mathbf{y}_t = [(1-s_t)(1-v_t),\ v_t,\ s_t] + \mathbf{e}_t$, with $\mathbf{e}_t$ Gaussian measurement error, where $(1-s_t)(1-v_t)$ is an idealized normalized open-water proxy (not a literal geometric area fraction) that decreases with both sediment encroachment and vegetation occupation, v_t represents vegetation index, and s_t is a storage proxy.

Two structural facts organize the result. First, the rate k does not appear in $\mathbf{y}$. A dynamically coupled rate could in principle be constrained indirectly through its covariance with observed states, subject to practical-identifiability limits (Walter and Pronzato 1997), but here we deliberately set the log-rate gain to zero. The independent latent-rate residual is therefore not learned from the condition observations. Second, in experiment configurations that retain the generic forcing c_t, k and c_t enter the removal law through their product, so they are structurally non-identifiable as separate factors (Bellman and Åström 1970). Recoverable performance is therefore the part that observable condition explains, and its complement is largely irreducible within the stated observing system.

Synthetic truth and observation operator

Two synthetic truths are used. An idealized truth isolates the inference mechanism, and a literature-parameterized simplified truth tests transfer to a more environmentally plausible parameterization; both are run over 120 monthly steps (10 years). Complete model equations, all parameter values with their literature or illustrative basis, the assimilation filter algorithm step by step, and a worked single-realization example (truth, open-loop, assimilation, and oracle) are provided in the Supplementary Material.

Idealized truth. The condition states evolve by prescribed dynamics that are illustrative of documented sediment accumulation, vegetation effects, and maintenance behavior rather than fitted to a site (Ahilan et al. 2019; Drake and Guo 2008; Erickson et al. 2018). Sediment storage fills through a flow-driven increment that accelerates as storage fills, because the denominator shrinks as s grows, and is capped at $s_{\max}$, $s_t = \min[s_{t-1} + a\,Q_t/(1 - s_{t-1} + b),\, s_{\max}]$, with $a = 0.011$, $b = 0.2$, and $s_{\max} = 0.92$, a fill law that treats normalized flow as a sediment-delivery proxy and is illustrative rather than a sediment mass balance; vegetation drifts upward as a genuine random walk, $v_t = \mathrm{clip}(v_{t-1} + 0.006 + \xi_t,\, 0.05,\, 0.95)$ with $\xi_t \sim N(0, \sigma_v^2)$ and $\sigma_v = 0.035$, whose month-to-month fluctuation the forecast cannot anticipate; and an unscheduled maintenance event at month 72 resets storage and vegetation ($s \to 0.10$, $v \to 0.40$) in the truth only, so the forecast model does not anticipate it. Flow is log-normal, $Q_t = \exp(N(0, 0.35^2))$, a dimensionless relative-flow multiplier with median one and arithmetic mean slightly above one, and temperature is seasonal. The hidden forcing declines linearly over the record, $c_t = \mathrm{clip}(1 - 0.55\,t/T,\, 0.45,\, 1.0)$, representing a stress scenario in which electron-donor support weakens; the dependence of wetland denitrification on carbon supply motivates that interpretation, not the imposed linear trajectory (Lu et al. 2009). In this notation the bare symbol $T = 120$ is the horizon, the record length in monthly steps, whereas the seasonal water-temperature factor carries a subscript, written T_t here and T_C in the literature-informed model, so T in t/T is not a temperature. Removal efficiency follows a first-order kernel, $\eta_t = \mathrm{clip}[0.90\,(1 - e^{-L_t}),\, 0,\, 0.95]$, in which the upper clip at 0.95 is not binding, since the ceiling here is 0.90, with a loading $L_t = k\,T_t\,c\,((1 - s)/Q)\,g(v)$ that couples the rate to temperature T_t, the hidden forcing c, remaining capacity $(1 - s)$, flow, and a vegetation-contact term $g(v)$ whose rising branch represents increasing vegetative drag followed by saturation, and whose falling branch is an illustrative stress representation of preferential routing around spatially heterogeneous dense vegetation rather than a fitted universal density-response curve (Min and Wise 2009; Nepf 2012; Sabokrouhiyeh et al. 2020) (full forms in the Supplementary Material). Here L_t is a dimensionless treatment-exposure number, a reaction-to-hydraulic-loading ratio and the analog of k/q, with the leading constants absorbed as scalings, where larger L means more reaction opportunity relative to hydraulic throughput, so only its relative variation carries meaning. Condition observations carry additive Gaussian noise of standard deviation 0.04 to 0.05 on the 0 to 1 scale.

Literature-informed simplified truth. The kernel is replaced by a k-C* treatment-wetland model combined with a tanks-in-series hydraulic representation (Kadlec and Wallace 2009; Merriman et al. 2017). The calculation prescribes a condition-derived effective tank count N_{eff} as an illustrative mapping rather than fitting the relaxed P parameter, and applies the resulting model to nitrate-nitrogen (Eq. 1).

$$\eta = \left(1 - \frac{C^*}{C_{\text{in}}}\right)\left[1 - \left(1 + \frac{k}{N_{\text{eff}}\,q}\right)^{-N_{\text{eff}}}\right], \qquad k = k_{20}\,\theta^{T_C - 20}\,c \qquad (1)$$

in which the effective number of tanks and the hydraulic loading are explicit functions of the observable state, $N_{\text{eff}} = 1 + 3(1-s)\,\tilde{g}(v)$, with $\tilde{g}(v) = \text{clip}(\text{contact}(v)/0.39,\, 0.3,\, 1.3)$ a normalized vegetation-contact factor, and $q = q_0\,Q/(1-0.6\,s)$. Here Q is the dimensionless relative-flow multiplier defined above and q_0 is the median-flow hydraulic loading. If A_0 is the nominal treatment area, the corresponding physical flow is $Q_{\text{phys}} = q_0 A_0 Q$; defining an effective treatment area $A_{\text{eff}} = A_0(1-0.6\,s)$ then gives $q = Q_{\text{phys}}/A_{\text{eff}} = q_0 Q/(1-0.6\,s)$. This is an illustrative mapping from sediment filling to reduced effective treatment opportunity rather than a literal loss of plan area, while $\tilde{g}(v)$ modulates hydraulic efficiency. In this model k is a first-order *areal* rate constant (velocity units, m/yr), distinct from the idealized dimensionless rate multiplier k of about 1.7 that absorbs scalings in the kernel above, so the carried log-rate is an effective rate multiplier whose physical interpretation depends on the kernel; C^* is the irreducible background concentration to which removal asymptotes; and N_{eff} is the effective number of continuously stirred tanks in series, a compact descriptor of hydraulic efficiency obtainable from a residence-time tracer study (Persson, J et al. 1999; Werner and Kadlec 2000). In plain terms N_{eff} is a dimensionless hydraulic-efficiency indicator, with $N_{\text{eff}} = 1$ a completely mixed tank and larger values approaching plug flow and indicating less short-circuiting. Its dependence on sediment and vegetation is an illustrative mapping from observable condition to hydraulic efficiency rather than a calibrated universal law. Parameter values combine literature-supported and illustrative choices. $C^* = 0.6$ and $C_{\text{in}} = 1.5$ mg/L are an illustrative high-nitrate scenario chosen to impose a 60% asymptotic removal ceiling; $k_{20} = 25$ m/yr is the reported median annual-average nitrate rate at 20 deg C (Kadlec 2012); $q_0 = 30$ m/yr is an illustrative median-flow hydraulic loading; and $\theta = 1.10$ is close to the reported modified Arrhenius factor of 1.106 for nitrate-removal wetlands (Kadlec 2012). Simulated removals span 2% to 53% (mean 16%), within reported stormwater ranges (Koch et al. 2014). Both the k-C* and tanks-in-series expressions form a monthly quasi-steady treatment model, not an event-scale hydrologic or biogeochemical mass-balance model; event-scale loading, bypass, and internal pools are future work.

Observation operator. In both truths, the observation vector is a function of condition only, $\mathbf{y}_t = [(1-s_t)(1-v_t),\, v_t,\, s_t] + \mathbf{e}_t$, with $\mathbf{e}_t \sim N(0, \mathbf{R})$ and $\mathbf{R} = \text{diag}(\sigma^2)$ the observation-error covariance, matched to the truth-generating noise. The open-water and vegetation channels represent established optical or radar retrieval targets, while the storage channel is an idealized remotely sensed footprint and storage-loss proxy whose assumed accuracy has not yet been demonstrated for this application; the removal efficiency η is never part of $\mathbf{y}$. The per-channel noise standard deviations (an absolute standard deviation of 0.04 to 0.05 on the normalized 0-1 scale) are a designed upper-bound OSSE error level for an idealized observing system, with surface water and vegetation broadly retrievable from satellite imagery (Huang et al. 2018; Pekel et al. 2016; Tucker 1979), although the same accuracy has not been demonstrated for an indirect storage-loss retrieval; $\mathbf{R}$ is diagonal (independent channels) and correctly specified, and the sensitivity of the results to the noise level is examined in the robustness analysis (Fig. S3).

Assimilation, calibration, and skill

At each month, the ensemble represents 400 plausible combinations of pond condition and latent rate. The model advances each member and converts it into the EO quantities that would be observed. Differences between the actual and predicted EO observations then correct storage and vegetation according to their forecast covariances. We deliberately prevent the observations from updating the independent latent-rate residual by setting its Kalman-gain row to zero. EO can nevertheless improve estimated removal because the corrected storage and vegetation enter the performance model directly and determine the prescribed condition-dependent portion of the rate.

Filter. Condition is assimilated with a stochastic (perturbed-observation) ensemble Kalman filter (Evensen 2003) of $N = 400$ members. We use a controlled synthetic OSSE in which the truth and the assimilation filter share the same condition and treatment functional kernels, while the assimilation filter represents unresolved process and latent-rate uncertainty and does not anticipate the maintenance reset. The open-loop and assimilation arms share initial ensembles and forecast random-number streams and differ only through the analysis update. A matched-structure sensitivity that varies the reactor form is examined separately (Fig. 4). Each member carries the condition states and, for the identifiability analyses, an augmented latent-rate ensemble whose propagated spread is deliberately excluded from analysis contraction and is not estimated from the observations, rather than a dual state-parameter update (Moradkhani et al. 2005). Each month proceeds in two steps. In the forecast step, every member is advanced by the process model with additive process noise. In the analysis step, each member's predicted observation $\mathbf{y}_i^f = h(\mathbf{x}_i^f)$ is formed, and the ensemble-estimated cross- and observation-covariances,

$$\mathbf{P}_{xy} = \frac{1}{N-1}\sum_i (\mathbf{x}_i^f - \bar{\mathbf{x}}^f)(\mathbf{y}_i^f - \bar{\mathbf{y}}^f)^\top, \qquad \mathbf{P}_{yy} = \frac{1}{N-1}\sum_i (\mathbf{y}_i^f - \bar{\mathbf{y}}^f)(\mathbf{y}_i^f - \bar{\mathbf{y}}^f)^\top + \mathbf{R} \tag{2}$$

give the Kalman gain and the perturbed-observation update,

$$\mathbf{K} = \mathbf{P}_{xy}\,\mathbf{P}_{yy}^{-1}, \qquad \mathbf{x}_i^a = \mathbf{x}_i^f + \mathbf{K}\,(\mathbf{y}_t + \varepsilon_i - \mathbf{y}_i^f), \qquad \varepsilon_i \sim N(0, \mathbf{R}) \tag{3}$$

with the updated states clipped to physical bounds. The log-rate row of the Kalman gain $\mathbf{K}$ is set to zero, a prescribed gain constraint, so condition observations do not update the rate; spatial localization is not needed at this state dimension.

Representing the unobserved rate. In configurations that retain the generic forcing c_t, it is not observed and enters only through the product $k\,c_t$. In the observability-budget experiment, the designed hidden residual z_h replaces this generic forcing; no additional declining c_t is applied. The latent rate is initialized and propagated with experiment-specific spread and jitter settings; its analysis gain is constrained to zero, so condition observations do not contract it, and Table S10 reports the controls used in each experiment. This encodes the observability structure directly. Assimilation refines the observable states, while the latent rate is propagated but not contracted by the observations. It also prevents the analysis from collapsing the performance band around an unobserved quantity, which would produce apparent but spurious skill.

Calibration. Two safeguards keep the comparison fair. The open-loop and assimilation arms share the same initial ensemble and forecast random-number streams, so their per-seed comparison is paired (Glasserman 2004); only the assimilation arm draws perturbed observations for the analysis update. The perfect-performance oracle is instead a deterministic point mass at the truth and does not use an ensemble random-number stream. The generative spread on the states and the rate is scaled so the open-loop 90% band covers the truth near 0.90 of the time, a covariance inflation calibrated to reliability; without this step an overconfident prior manufactures apparent contraction. The controls are experiment-specific. Aging uses separate state- and rate-spread controls to target storage and performance coverage, respectively; the observability-budget experiment instead calibrates one global ensemble-spread inflation; and the matched-structure and maintenance experiments use the controls listed in Supplementary Table S10. Thus, before assimilation, the ensemble spread is calibrated toward 90% open-loop coverage on training seeds, and the reported recovery is what assimilation adds on top of that baseline. All arms are then evaluated on disjoint held-out seeds, with paired per-seed uncertainty for the open-loop versus assimilation comparison. Because the rate is excluded from the observation operator and its gain row is zero, condition innovations cannot identify the hidden rate, so setting its prior would require performance data, informative priors, or hierarchical transfer from an instrumented cohort rather than the assimilation filter's own innovation statistics.

Skill metric. Performance recovery is measured with the continuous ranked probability score (CRPS), a proper score sensitive to both ensemble calibration and sharpness, which for an N-member ensemble $\{x_i\}$ and truth y is

$$\mathrm{CRPS} = \frac{1}{N}\sum_i |x_i - y| - \frac{1}{2N^2}\sum_i\sum_j |x_i - x_j| \qquad (4)$$

(Gneiting and Raftery 2007; Hersbach 2000). CRPS rewards a forecast for being both sharp and centered on the truth and penalizes a narrow but incorrect band, so an assimilation filter that narrows overconfidently does not gain skill. Recovery is reported as the proper-score skill B_S. In general form,

$$B_S = \frac{S_{\text{open}} - S_{\text{assim}}}{S_{\text{open}} - S_{\text{oracle}}}, \qquad S = \mathrm{CRPS} \qquad (5)$$

where S_{open}, S_{assim}, and S_{oracle} are the per-step-averaged CRPS of the open-loop, assimilated, and oracle performance forecasts. The oracle is a perfect-performance oracle, a point mass at the true efficiency, which sets the denominator. In the special case where the oracle CRPS is zero, that is, where the reference collapses to the true performance, B_S reduces to the CRPS-skill fraction $1 - S_{\text{assim}}/S_{\text{open}}$. We report B_S on a percentage scale throughout. A value of B_S is a predictive-skill percentage, the fraction of the CRPS gap between the open-loop and perfect-information forecasts that assimilation closes; it is not a fraction of nitrogen mass removed, of removal efficiency, of performance variance, or of a regulatory load-reduction credit. The coverage of the truth by the posterior band is reported alongside as a calibration check. Absolute CRPS values and the coverage fields are reported in the Supplementary Material. The observability-budget map (Fig. 2) reports B_S accompanied by the coverage field so that overconfident cells are identifiable, and credible-interval width reduction is retained only as a diagnostic because it can reward overconfident narrowing.

Observability-budget, aging, and maintenance experiments

Three experiment families quantify the framework; the full model and assimilation settings are listed in Table 1, with complete configurations in the Supplementary Material.

Observability-budget experiment. The log removal-rate variation is written as a designed-share sum of an observable-vegetation term, an observable-sediment term, and a hidden residual, $\sqrt{\alpha_v}\, z_v + \sqrt{\alpha_s}\, z_s + \sqrt{\alpha_h}\, z_h$, where z_v is a standardized vegetation-derived signal, z_s a standardized sediment-derived signal, z_h a causal hidden first-order autoregressive series generated independently of the observable signals, and $\alpha_v + \alpha_s + \alpha_h = 1$. In this experiment, this designed-share modifier replaces the generic declining forcing c_t used in the idealized truth; no separate c_t multiplier is applied, so z_h is the only hidden rate driver in the budget decomposition. The observable signals are standardized on a population law without truth-trajectory look-ahead, and the coefficients $(\alpha_v, \alpha_s, \alpha_h)$ are designed (expected) variance shares; because the population-scaled observable signals carry a modest per-realization cross-covariance, the realized variance and covariance decomposition is reported in the Supplementary Material. The shares partition variation in the log-rate modifier rather than in total removal efficiency, since observed condition still enters the removal kernel directly. The latent-rate ensemble the assimilation filter carries is scaled with the hidden share, with no residual floor, so the $\alpha_h = 0$ edge is fully observable for the inference system. The designed expected, or population-level, amplitude is held fixed so that only the observability of the rate, not its magnitude, changes across the sweep. The assimilation filter is given the observable relationship, while the independent hidden residual remains unupdated because the log-rate gain is zero; sweeping α_v and α_s over the simplex maps recovered performance against the observable share (Fig. 2). The vegetation random-walk scale σ_v is treated as a designed stress scale, and the observability budget's sensitivity to it, together with a forcing-uncertainty sensitivity, is reported with the results.

Aging-mechanism experiment. Six mechanisms by which sediment fill degrades performance are compared, each expressed as an explicit modifier of the removal kernel. The six mechanisms are capacity loss (the capacity factor scales as $1-s$); rate suppression (the rate scales as $1-0.7\,s$); hydraulic short-circuiting (the effective tanks decline, $N_{\text{eff}} = 1 + 2(1-s)$); residence-time loss (a milder capacity factor, $1-0.6\,s$); internal loading (capacity loss plus an empirical net-export penalty that subtracts removal above a fill threshold, used to allow negative net removal rather than a mechanistic sediment nutrient-flux model); and a combined case (capacity, rate, and short-circuiting together). Each mechanism is independently calibrated to open-loop coverage near 0.90, and recovery is scored with the same proper-score skill B_S, to test whether recovery depends on the mechanism.

Maintenance experiment. A single pond is simulated over a 240-month (20-year) horizon with variable log-normal sediment loading, so the storage-fill rate differs from year to year. The single unanticipated month-72 event in the 120-month truth resets both storage and vegetation, whereas this 240-month maintenance experiment models dredging that resets storage only, and they are separate illustrative experiments. Maintenance (dredging) resets storage; the due condition is a storage-fill threshold s^* (baseline 0.5), the preventive-maintenance trigger. Four policies decide when to dredge. They are a fixed calendar (every 60 months); periodic inspection (every 24 months, consistent with the EPA one-to-three-year guidance, dredging when a noisy field measurement exceeds s^*); EO assimilation (a monthly noisy condition observation is assimilated by a sequential assimilation filter on storage, dredging when the estimate exceeds s^*); and a perfect-information oracle (the true storage is known). Nitrogen removal declines with fill, $\eta(s) = \eta_{\max}(1 - s/s_{\text{fail}})$, where s_{fail} is the assumed functional-failure level, and is never observed by any policy. Policies are scored on disjoint held-out seeds, with the storage assimilation filter's spread calibrated to open-loop coverage near 0.90 on training seeds as in the other experiments and outcomes reported as means with standard errors, which throughout are across-replicate Monte Carlo standard errors conditional on the assumed model and parameters, not field-calibrated confidence intervals or a measure of structural uncertainty, on the fraction of time the pond is above the maintenance threshold (threshold-exceedance exposure), a mean removal-efficiency proxy (the time-averaged efficiency, not load-weighted mass removed), and the number of interventions. Structural robustness (reactor form and kinetics) and maintenance parameter sensitivity are reported with the results (Figs. 4 and 6).

Table 1. OSSE model and assimilation settings.

Setting	Value
Monthly steps; unscheduled maintenance event	120; step 72 (truth only)
Ensemble size	400 (condition experiments); 300 and 200 (maintenance baseline and sensitivity)
Replicates	10 to 40 (per experiment)
Assimilated state	$[s, v]$; effective log-rate carried with prescribed hidden-forcing spread, gain row set to zero, not observation-updated
Observation-noise SD (condition channels)	0.04, 0.05, 0.05 (correctly specified $\mathbf{R}$)

Setting	Value
Generative-spread calibration	open-loop coverage near 0.90 on training seeds; per-experiment controls (Supplementary Material); evaluation on disjoint held-out seeds
Effective-rate spread	experiment-specific (Supplementary Material, Table S10); latent rate carried with zero analysis gain, observability-budget latent spread scaled with the hidden share
Literature-informed synthetic truth (nitrate-N)	k-C* tanks-in-series; $k_{20} = 25$ m/yr; $q_0 = 30$ m/yr; $C^* = 0.6$, $C_{\text{in}} = 1.5$ mg/L; $\theta = 1.10$
Maintenance horizon	240 months (20 yr); variable log-normal sediment loading
Maintenance policies	calendar (5 yr); inspection (2 yr); EO assimilation (monthly); oracle

Results

The observability budget on held-out seeds

Assimilating condition appears to constrain the observable states well while recovering rate-driven performance according to how much of the rate is explained by observable condition. Partitioning the rate variation into a designed observable-vegetation share, an observable-sediment share, and a hidden residual yields a single map (Fig. 2), evaluated on disjoint held-out seeds. The three shares $(\alpha_v, \alpha_s, \alpha_h)$ are designed (expected) variance fractions rather than exactly realized ones; the realized variance and covariance decomposition is reported in the Supplementary Material, where the observable axes carry a modest realized cross-covariance. These shares partition the variation in the log-rate modifier, not the total variation in removal efficiency, because observed storage and vegetation still enter the removal kernel directly even when the rate modifier is fully hidden. Recoverable performance, measured as the proper-score skill B_S, appears to rise broadly with the observable share $\alpha_v + \alpha_s$. Where the rate modifier is fully hidden, B_S is only about 16%, with the open-loop band well calibrated (coverage near 0.87); this residual recovery comes from the direct condition pathways rather than from learning the hidden rate. Through the partly hidden interior, B_S climbs to roughly 40% at a nominal even mix (about 0.4 vegetation, 0.4 sediment, 0.2 hidden). Along the fully observable edge, where the rate modifier is entirely explained by observed condition, B_S reaches about 65% to 76%. These fully observable cells are sharp and overconfident, however, with open-loop coverage near 0.60, so they are flagged rather than read as calibrated. Nine of the twenty-one cells fall inside the acceptance band $[0.85, 0.95]$, concentrated among the hidden-dominated and intermediate cells; open-loop coverage declines as the observable share grows, reaching about 0.60 at the fully observable edge. The map therefore suggests that hidden-rate performance is recovered only weakly, about 16% when the rate is fully hidden, and that recovery grows with the observable share, becoming large but overconfident where the rate is fully observable under the known-forcing idealization. Because the log-rate gain is held at zero, this is recovery through better estimation of observed condition under a prescribed no-rate-learning assimilation filter rather than learning of the latent rate itself, and B_S can in principle be negative where assimilation degrades the forecast. The next section indicates that the edge overconfidence reflects the assumption of perfectly known forcing rather than the recovery estimate.

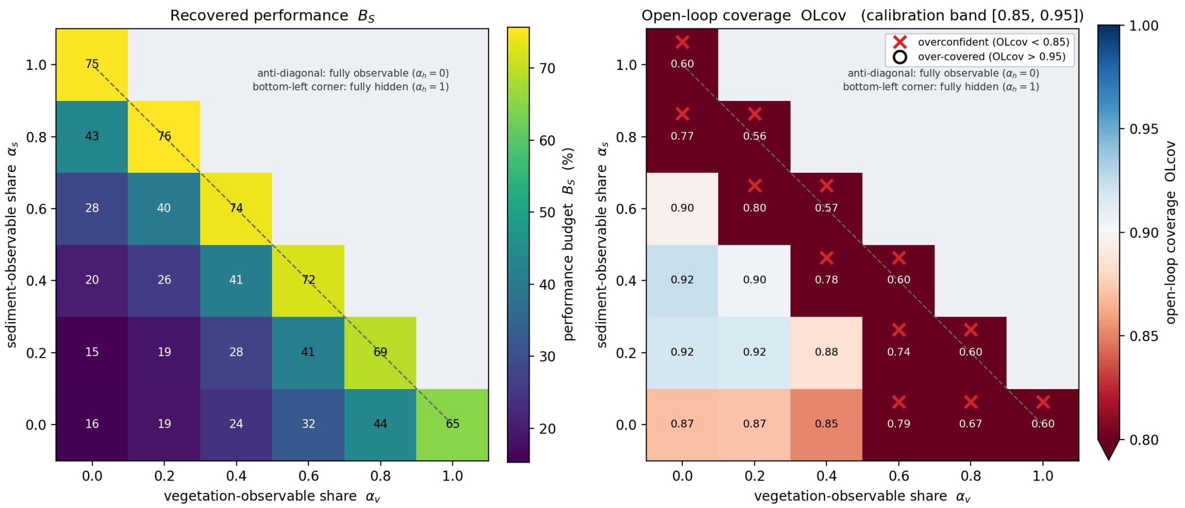

Fig. 2. Observability-budget map, held-out seeds. Axes are the designed fraction of removal-rate variation attributed to observable vegetation and to observable sediment; the hidden share is $1 - \alpha_v - \alpha_s$. Panel A prints the recovered performance, the proper-score skill B_S (normalized CRPS reduction, in percent, a predictive-skill percentage rather than a fraction of nitrogen removed), which rises with the observable share from about 16 at the fully hidden corner to about 65 to 76 along the fully observable edge. Panel B prints the open-loop coverage; cells outside the acceptance band $[0.85, 0.95]$ are marked (overconfident or over-covered). Coverage is near 0.90 among the hidden-dominated cells and declines as the observable share grows, reaching about 0.60 at the fully observable edge; nine of the twenty-one cells fall inside the band. Assimilation coverage is reported in the Supplementary Material.

The overly narrow uncertainty bands along the fully observable edge appear to come from a simplification in the experiment: the model is handed the exact flow and temperature, as if these inputs were known without error. When we instead let each ensemble member use a slightly different flow and temperature, scattered around the true values rather than fixed at them, the B_S at the edge barely changes, but its uncertainty bands widen to a more honest width. Adding about 15% scatter in flow and about 1 °C in temperature leaves the sediment-driven edge B_S near 74%, down from about 75%, while the fraction of time the true performance falls inside the predicted band rises from about 0.71 to about 0.85, back into the acceptable range. A larger 30% flow scatter lowers the edge B_S only slightly, to about 71%, and pushes that fraction to about 0.96. The vegetation-driven edge is nearly unchanged, and the mostly-hidden middle of the map is unaffected by input scatter, as expected, since there the performance swings are governed by the unobserved removal rate rather than by flow or temperature. Because this test only adds random scatter around the correct flow and temperature, the edge bands are best read as a best case that widens to an appropriate width once realistic input uncertainty is admitted. It does not test flow or temperature that is systematically biased (consistently too high or too low), which we would expect to hurt more and leave to future work.

Recovery of storage-driven aging performance

When sediment fill degrades performance by acting through the storage state we observe, recovery is strong, because storage is observed. We varied the aging mechanism and scored recovery with the same proper-score skill B_S on held-out seeds, and recovery tracks how much each mechanism works through observable condition (Fig. 3). Internal loading recovers most, at about 68%, followed by rate suppression at about 55%, then capacity loss and residence-time loss at about 49% to 50%, and the realistic combined case at about 40%. Hydraulic short-circuiting recovers least, at about 24%. Two calibration notes apply. Across mechanisms, the open-loop bands contain the truth about 0.83 to 0.99 of the time and the assimilated bands about 0.99 to 1.00, so the assimilated bands are wider than they need to be; we flag this as a caveat on the exact values, without assuming which way a recalibration would move them. Storage itself is recovered consistently across every mechanism, at a skill near 90%, which appears to be why the storage-driven mechanisms recover best. That 90% is measured against an open-loop storage forecast whose bands are too narrow on the held-out seeds (storage coverage about 0.67, rising to about 0.92 once condition is assimilated), with the state-spread setting at the top of the tested range, so we read it as indicative rather than exact. In short, the two experiments measure different things: the observability-budget experiment measures hidden-rate recovery, which grows with the observable share, while this one measures storage-routed recovery, which is strong because storage is observed, and we keep them separate rather than merging them into a single range.

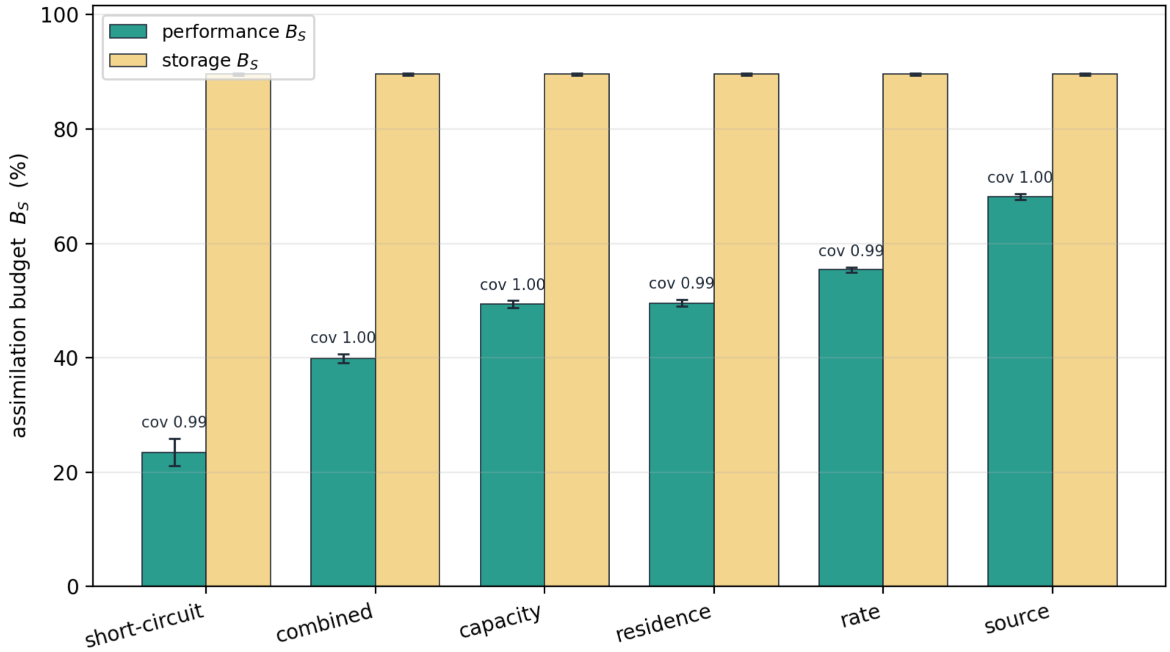

Fig. 3. Recovered performance by aging mechanism, proper-score skill B_S (normalized CRPS reduction over open-loop, the same metric as Figs. 2 and 4) on held-out seeds. Recovery scales with how much each mechanism routes performance through observable condition. Paired bars show the storage recovery, consistent across mechanisms at a proper-score skill near 90%, measured against an underdispersed open-loop reference (storage coverage about 0.67 open-loop and 0.92 assimilated), so this magnitude is indicative rather than fully reliability-controlled. Error bars are the across-seed standard error.

Matched-structure sensitivity

The observability-budget result appears to be a structural property of the problem, not an artifact of the one reactor form we happened to choose. To check this, we repeated the experiment with the assimilation filter and the truth using the same reactor form, and with the removal rate left hidden (its observation update turned off), across five common forms: a single well-mixed tank ($N = 1$), three tanks in series ($N = 3$), near-plug-flow ($N = 8$), an exponential kernel, and a k-C* form with an effluent floor. Scored on held-out seeds with the same skill measure B_S, recovery of the hidden, rate-driven performance was near zero in every case, ranging from about -13% to $+1\%$. The small negative values mean that in those runs assimilation slightly worsened the performance forecast rather than simply failing to help it. Recovery of the storage (sediment accumulation) level was also small in these runs (about 2.5%, against a poorly calibrated reference), with one exception: the compounded-aging case, where aging works by filling storage, so the observable sediment accumulation carries the signal and storage recovery jumps to about 80%. We read this figure qualitatively, for the pattern rather than the exact bar heights, because here a single knob sets the spread of both the condition and the rate ensembles at once, unlike the two separate knobs used elsewhere, and how well-calibrated the results are varies across the reactor forms (the performance bands here are too wide). The qualitative conclusion is nonetheless clear and matches the main result: assimilating condition does not improve hidden, rate-driven performance for any of the reactor forms tested when the rate is left unobserved. Note that this test keeps the assimilation filter and the truth matched to the same reactor form; it does not test what happens when the assimilation filter assumes the wrong form, which would be a harder case.

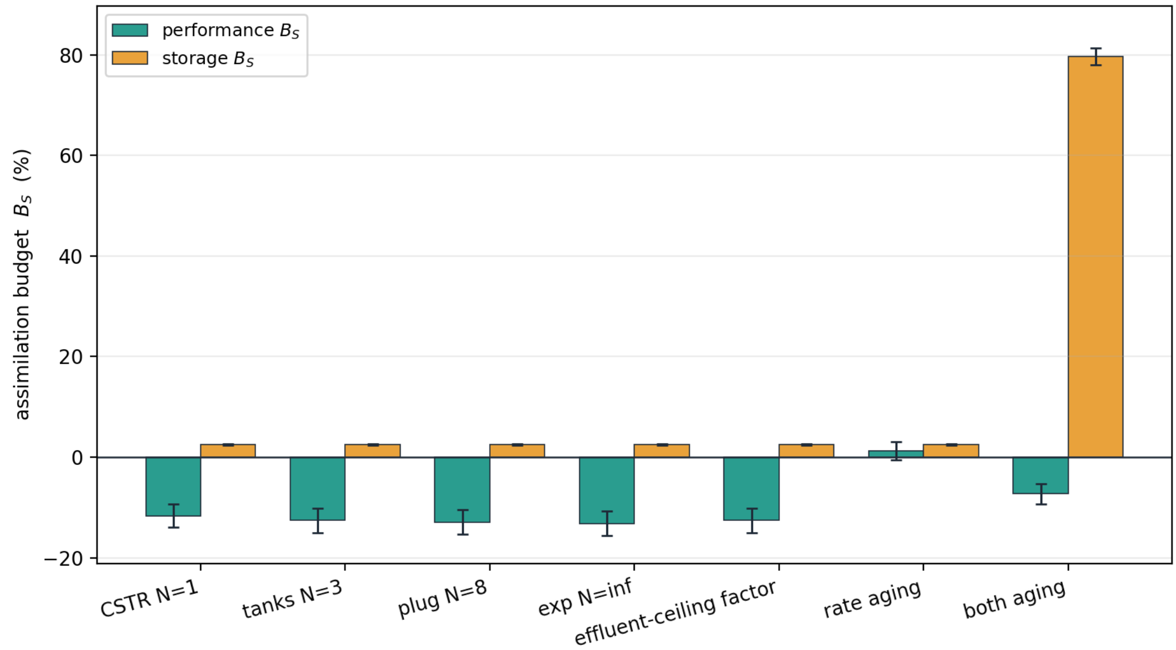

Fig. 4. Matched model structure sensitivity. Across reactor structure ($N = 1$, $N = 3$, $N = 8$), kinetic form (exponential kernel), and a k-C* effluent-ceiling factor, condition assimilation does not recover hidden-rate-driven performance under a zero-gain rate; paired bars report the performance and storage proper-score skill B_S per scenario, the same metric as Figs. 2 and 3. Performance recovery is near zero or negative (forecast degradation), and storage recovery is small in these hidden-rate structures. Because a single spread parameter scales the state and rate ensembles together here, this sensitivity is read qualitatively rather than as a calibrated magnitude comparison. The last group is the compounded-aging case, in which storage is routed into performance, so storage recovery is high (near 80%) while performance recovery stays near zero or negative. Error bars are the across-seed standard error.

Robustness of the observability budget to the vegetation stress scale

One reasonable worry is that our recovery numbers depend on a modeling choice we made: how much the vegetation is allowed to wobble unpredictably from month to month. We set that wobble with a single knob, σ_v, which we treat as a chosen stress level rather than a value tuned to make the results look good. To check that the observability budget does not hinge on it, we re-ran the experiment across a plausible range of the wobble, from small ($\sigma_v = 0.01$) to large ($\sigma_v = 0.05$). The proper-score skill B_S at the fully observable, sediment-driven corner barely changed, staying at about 70% to 77% (the same as the fully observable edge in Fig. 2), and it did not climb or fall steadily with the wobble; it peaked near $\sigma_v = 0.02$. Our working value of $\sigma_v = 0.035$ therefore sits in the middle of the tested range, not at a favorable extreme that would flatter the result. Recovery in the mixed, partly hidden interior of the map stayed low throughout. In short, the observability budget is set by how much of performance is observable, not by how much month-to-month vegetation noise we assumed.

Recovery is driven by the prescribed hidden share, not the assimilation filter prior

A sharper worry is that the recovery we report simply reflects what we told the assimilation filter to assume about the hidden rate, rather than anything physical. Two things could in principle drive it: a physical fact, namely how much of the removal rate is genuinely hidden versus visible, or a modeling choice, namely how much hidden-rate uncertainty we hand the assimilation filter to begin with. This second possibility is a real concern because the assimilation filter is never allowed to learn the hidden rate; it simply carries whatever hidden-rate uncertainty we assign, and that assigned uncertainty sets a floor on the performance band that no observation can reduce. Telling the filter the hidden rate is very uncertain therefore makes recovery look small, while telling it the rate is nearly certain makes recovery look large, even though the pond itself has not changed. In any single run the physical fraction and our assigned uncertainty are thus confounded, since both widen or narrow the performance band, so we separate them with two sweeps that each vary one while holding the other fixed. Both use the same tanks-in-series model in the truth and the assimilation filter and standardize the signals on population statistics rather than by peeking at each simulated trajectory. In the first sweep we varied the physical quantity, raising the truly hidden fraction of the rate from 20% to 80% while keeping the overall size of the rate swings the same and telling the assimilation filter the correct amount of hidden uncertainty at each level; B_S fell steeply, from about 44% to about 5%, while the bands stayed well-calibrated (coverage 0.87 to 0.92), so this decline can only come from the hidden fraction itself. In the second sweep we varied the modeling choice, holding the pond fixed and instead changing what the assimilation filter assumed about the hidden-rate uncertainty; B_S barely moved, staying near 20% to 28% with a gentle peak, and only an unrealistically tight assumption was penalized as overconfident bands, so the well-calibrated setting sits in the middle of the range. Taken together, B_S is controlled by how much of performance is genuinely hidden, not by how we tuned the assimilation filter, which is what lets us read the observability budget as a property of the observing system and the process rather than of the assimilation filter's settings.

EO assimilation may enable near-oracle preemptive maintenance within the tested rule class

Condition is recovered well across the mechanisms we examined, which points to a practical use. In the maintenance experiment, on held-out seeds, EO assimilation tracks storage better than a no-assimilation baseline, with a storage B_S of about 35% (a tracking score measured at the known dredging times, separate from the policy comparison below). The open-loop band is well-calibrated, containing the truth about 89% of the time, while the assimilated band is a little too narrow (about 79%). The estimated storage is accurate enough to call for dredging close to the true threshold crossing, coming near the oracle, a benchmark that knows the true storage exactly, on every measure. It delivers about 99.6% of the oracle's average removal efficiency (a time-averaged efficiency, not pollutant mass removed), dredges about as often as the oracle (roughly 3.5 times in 20 years), and leaves the pond over the dredge threshold only about 1.5% of the time (Fig. 5). The two current-practice methods do worse in this synthetic experiment. Periodic inspection dredges too rarely, leaving the pond over the threshold about 16% of the time and delivering about 7% less removal, because it cannot see the pond between inspections. A fixed calendar cannot adapt to year-to-year swings in sediment delivery, so in high-loading years it sits over the threshold about 3% of the time while dredging a similar or smaller number of times. This pattern holds even though the actual removal is never observed, because the dredging decision needs only condition, which is the part we can recover. Finally, the oracle here is a threshold rule with perfect knowledge of storage, not a cost-optimized policy, so the comparison shows how good threshold-triggered dredging can get, not the best possible maintenance strategy.

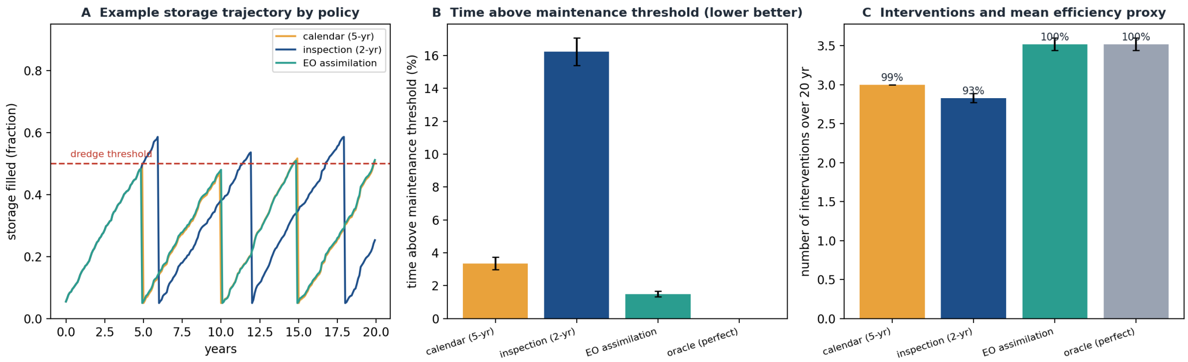

Fig. 5. Maintenance policy comparison over 20 years with variable loading, held-out seeds. (A) Example storage trajectory by policy against the dredge threshold. (B) Threshold-exceedance exposure with standard-error bars (lower is better). (C) Number of interventions over 20 years, with the mean removal-efficiency proxy (percent of oracle) annotated. EO assimilation approaches the perfect-state threshold oracle within the tested rule class, while periodic inspection under-maintains and the fixed calendar cannot adapt to variable loading.

Maintenance robustness

The maintenance advantage holds up as we vary the operating conditions (Fig. 6). We swept five of them: the dredge threshold, how fast the pond fills with sediment (the aging speed), how much the sediment loading varies from year to year, the inspection interval, and the observation noise. Across all of these, EO assimilation keeps the pond over the threshold only about 0.7% to 2.1% of the time (close to the perfect-knowledge oracle) and delivers about 99.6% to 100% of the oracle's average removal efficiency. Periodic inspection does worse, leaving the pond over the threshold about 3% to 30% of the time and removing somewhat less. The fixed calendar is the most fragile under fast aging: when an unmaintained pond would reach the threshold in just three years, the calendar leaves it over the threshold about 39% of the time. These results apply to the tested threshold-triggered policies and to a simple straight-line relationship between fill and efficiency, whose realism we address in the limitations below.

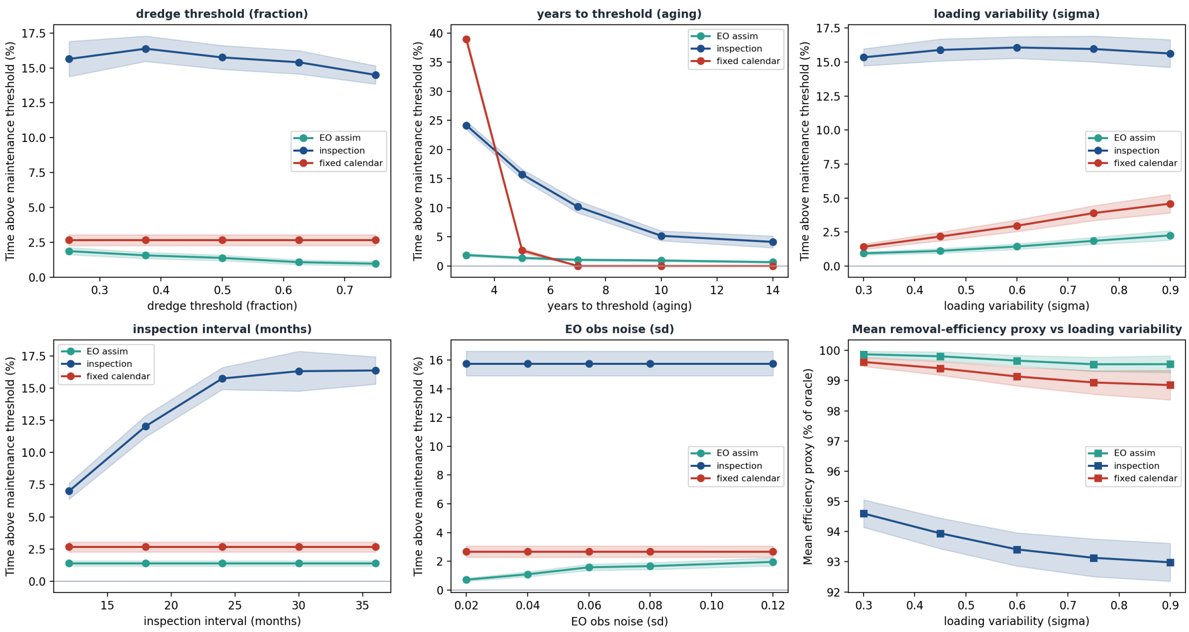

Fig. 6. Maintenance sensitivity across operating parameters, held-out seeds with standard-error bands. EO assimilation stays near the perfect-state threshold oracle (low threshold-exceedance) across every swept parameter, while periodic inspection consistently under-maintains and fixed calendar scheduling is fragile under fast aging.

Discussion

The results give a graded answer to what EO might deliver for monitoring BMP, particulary wetlands and ponds. Condition is recovered well. Removal performance is recovered only in the amount set by the observability budget, which is the share of the attainable forecast improvement that assimilating condition actually delivers for a given observing system, process model, prior, and forcing. On held-out seeds that share is about 16% where the removal rate is fully hidden, and it rises with the observable share to about 65 to 76% where the rate is fully explained by observed condition, although those fully observable cells are likely overconfident, so they are better read as a best case. Where aging degrades performance through the observed storage, recovery is larger, from about 24% to 68%, because storage is observed, and storage itself is recovered at a B_S near 90%. The two experiments measure different things, and we report them separately rather than merging them. Where the rate is genuinely hidden, the part we do not recover is a gap that no amount of additional EO imagery can close on its own; closing it requires information the satellite sensor currently does not carry. That turns the hope of monitoring treatment performance from space into a design question. For a given asset class, what is the observability budget, and where does a given asset sit within it?

For monitoring-network design, the observability budget could inform how effort is allocated rather than prescribe it. Ponds whose removal rate is largely governed by observable condition could be tracked from space with real skill, while ponds governed by hidden biogeochemistry would still need field measurement. Which case a pond falls into should depend on what limits denitrification there. Where nitrate removal is limited mainly by contact, so that the binding constraints are residence time, remaining storage, and plant contact, the rate follows quantities imagery may help constrain and the budget should be high (Kadlec and Wallace 2009; Nepf 2012; Sabokrouhiyeh et al. 2020; Werner and Kadlec 2000). Where nitrate removal is limited instead by electron-donor supply or redox, as would be expected in catchments delivering little labile organic carbon, the rate rides on the hidden forcing, two ponds that look alike from space can perform very differently, and the budget should be low (Bachand and Horne 1999; Kadlec

2012; Lu et al. 2009). These are expectations to be checked against field data rather than results, since our simulation prescribes the observable and hidden shares rather than measuring them at real assets. In practice the budget would have to be measured rather than assumed, because in this simulation we set the observable and hidden shares ourselves. A small set of instrumented sites could give first estimates of how much of the rate variation observed condition explains, and process understanding could extend those estimates to similar assets. Because the hidden rate is likely not recovered directly from the observations, the assimilation filter cannot learn it from imagery alone, so filling the budget would require performance measurements, informative priors, or borrowing strength from instrumented sites of the same class. Assembling the benchmark performance data that this depends on is arguably the binding constraint on operational EO monitoring of stormwater assets (Kumar 2026). The recoverable share is therefore something targeted monitoring investment could enlarge, and measuring it is the first step toward that investment. This suggests a simple decision structure for an asset class. The first step is to estimate its observability budget from a small instrumented cohort. If the budget is high, most of the performance variation is routed through condition, EO assimilation can carry much of the monitoring load, and field effort can be reserved for periodic checks. If the budget is low, the next question is why, because two very different problems produce the same symptom. If condition itself is poorly retrieved, the gap is a retrieval problem, and the investment belongs in better condition products, such as finer resolution or a validated storage-loss retrieval. If condition is retrieved well but performance still does not follow it, the gap is a hidden-rate problem that no improvement in imagery can close, and the investment belongs instead in a field-instrumented cohort (with occasional inflow and outflow sampling, tracer studies, or redox and sediment-chemistry measurements) whose measurements can be transferred to similar assets. Separating these two cases matters, because they call for opposite spending decisions.

The observability budget also bears on how performance is credited. Some load-accounting and nutrient-credit frameworks assign standardized, type-based removal efficiencies rather than time-varying, asset-specific values (Commonwealth of Virginia 2024; U.S. Environmental Protection Agency and Chesapeake Bay Program 2003). The budget indicates where that practice might eventually give way to a condition-informed, time-varying credit and where it could not. For an asset class with a high budget, an EO-informed estimate could carry information about performance beyond the static category value. For a class with a low budget, an EO-derived performance number would mostly reflect the prior rather than the asset, so a standardized credit with periodic field verification would remain more transparent. The same reasoning supports triage under a fixed inspection budget, since EO could screen a population for condition while field crews are sent to classes with a low budget or to assets whose condition has departed from expectation. We offer this as a research direction rather than a regulatory recommendation, because it presumes validated EO condition products and a field-estimated budget that this study does not supply.

The maintenance result does not have to wait on filling the observability budget. Condition is recovered whatever the observation budget turns out to be, so EO assimilation could support condition-based maintenance that keeps ponds below the dredge threshold and protects removal. In the simulation it matched a threshold rule that knows the true storage, and it beat the fixed-schedule and infrequent-inspection approaches we tested. The apparent value is largest precisely where fixed schedules fail, under variable sediment loading, where the timing of capacity loss is unpredictable. Because the decision needs only condition, the same logic would extend from one pond to a portfolio, although we simulate a single pond here. An agency with more ponds than dredging capacity could rank its assets by estimated storage and schedule the few that are actually approaching the threshold, instead of running a fixed rotation that is early for some ponds and late for others. That ranking should matter most where sediment delivery varies between sites and between years, which is where a fixed rotation carries the least information. Using this in the field would require validation first, including EO condition products checked against ground data, and field testing. In this demonstration EO enters as an idealized monthly measure of storage-related condition, which is a best case for an observing system, and no monthly retrieval of hydraulic storage loss has yet been validated at the accuracy we assume.

Limitations and future work

The findings here are properties of a simulated system studied under stated assumptions, and each is best read as a hypothesis to be tested rather than an established measurement. Our observing system sees condition directly every month with small, independent errors, and it treats three observation channels as independent even though they carry only two independent pieces of information, so it should be read as a best case. A more plausible observation model could add an indirect storage retrieval, since storage loss is not directly sensed, along with correlated channel errors, a realistic revisit cadence with cloud and seasonal gaps, mixed pixels and registration error, and persistent retrieval bias. Small ponds are especially challenging for medium-resolution imagery. Sentinel-2 provides 10-m bands suitable for many surface-mapping applications (Drusch et al. 2012), but recent pond-inventory research shows that conventional satellite mapping has difficulty resolving small ponds and motivates size-adaptive, multi-sensor methods (Liu et al. 2024). For the smallest assets, shoreline pixels may mix water, vegetation, and surrounding land, leaving few uncontaminated interior pixels. Finer commercial small-satellite imagery can improve spatial and temporal sampling in aquatic applications (Li et al. 2022), but its demonstrated coastal-turbidity retrieval should not be taken as validation for stormwater-pond condition or storage. Radar can reduce cloud limitations but measures a different quantity. The storage channel remains the weakest link, because sediment accumulation changes bathymetry, which neither ordinary optical nor radar imagery observes directly. A validated storage-loss retrieval would therefore likely require repeat lidar, drone photogrammetry, or an indirect inference from open-water area and shape, each carrying its own error budget that this study does not represent. Flow and temperature, treated here as known inputs, may in practice be as uncertain as condition. Each of these limitations would be expected to lower recoverable skill relative to observing the states directly.

In the maintenance experiment, removal efficiency is a fixed function of storage, so once storage is known the performance follows exactly, and the near-oracle result may partly reflect that. This experiment is a demonstration, and making it realistic is future work. That work could add hidden biogeochemistry and hidden rate variability, so that knowing storage no longer pins down performance; score the mass of nitrogen removed rather than the time-averaged efficiency, which would give weight to the wet periods when most of the load arrives; compare against a policy that triggers on raw EO with no assimilation at the same observation frequency; choose the best fixed interval in advance rather than assuming five years; and add an explicit cost function. The oracle here is a threshold rule that knows the true storage, not an optimal policy, so it shows the ceiling for threshold-triggered dredging rather than the best achievable maintenance.

Conclusions

Whether EO can tell us how well a distributed BMP is removing nitrogen is an observability-budget question. Scored properly and on held-out seeds, assimilating observed condition recovers performance in proportion to how much of that performance runs through condition the sensor can see, and little beyond it. Where performance rides on a hidden rate, the observability budget, measured as B_S, the share of the gap to a perfect-knowledge forecast that assimilation closes, is about 16% when the rate is fully hidden and rises with the observable share to about 65 to 76% when the rate is fully explained by observed condition, although those fully explained cells are overconfident because the experiment supplies the true flow and temperature, and are best read as a best case. Where aging degrades performance through the observed storage, the budget is larger, from about 24% to 68%. Storage itself is recovered strongly in the aging experiments and moderately in the separate maintenance tracking check, which is evaluated at the known dredging times and reported apart from the policy comparison, with calibration caveats noted. Because the dredging decision needs only condition, EO assimilation can support preventive maintenance that comes close to a rule with perfect knowledge of storage, within the threshold-triggered policies we tested, and that helps protect the removal the sensor never sees. We propose the observability budget as a design quantity. It indicates what present-day EO might recover under these assumptions, and it points to the calibration and benchmark data that could recover more. The framework is developed for nitrogen and may extend to other pollutants whose removal is governed by condition, which we offer as a hypothesis rather than a demonstrated result.

Data Availability Statement

All data, models, and code generated or used during the study are publicly available at https://github.com/skp703/observability-budget-osse, in accordance with ASCE's data-sharing policy. The repository contains the idealized and literature-informed OSSE implementations, the observability-budget, aging, maintenance, structural-sensitivity, and parameter-sensitivity drivers, and the figure-generating scripts, from which all reported numbers and figures regenerate.

Appendix. Notation

The following symbols are used in this paper:

C^* = background (irreducible) concentration (mg/L); C_{in} = influent concentration (mg/L); c = hidden biogeochemical forcing; $\mathbf{e}$ = observation error; k = removal rate, a dimensionless multiplier in the idealized kernel and a first-order areal rate constant (m/yr, reported as k_{20}) in the literature-informed kernel; $\ln k$ = natural-log effective rate multiplier, the augmented state; $\mathbf{K}$ = Kalman gain (log-rate row set to zero); N = ensemble size; N_{eff} = effective number of tanks in series; $\mathbf{P}_{xy}$, $\mathbf{P}_{yy}$ = cross- and observation-covariances; Q = flow; q = hydraulic loading rate (m/yr); $\mathbf{R}$ = observation-error covariance; S = per-step-averaged CRPS of a forecast arm; $S_{\text{open}}, S_{\text{assim}}, S_{\text{oracle}}$ = CRPS of the open-loop, assimilated, and oracle arms; s = sediment-induced storage-loss fraction; s^* = preventive-maintenance trigger (dredge threshold); s_{fail} = assumed functional-failure level; T = time horizon (number of monthly steps); T_t = seasonal temperature factor; t = time step; v = vegetation density; $\mathbf{x}$ = state vector; $\mathbf{y}$ = observation vector; $\alpha_v, \alpha_s, \alpha_h$ = designed observable variance shares (vegetation, sediment, hidden residual); β = loading coefficient; ε = observation-perturbation draw; η = nitrate-nitrogen removal efficiency; $\lambda_{\text{state}}, \lambda_{\text{rate}}$ = state- and rate-spread calibration scalars; μ_v = vegetation drift; ξ_t = vegetation random-walk noise; σ_v = vegetation random-walk standard deviation (designed stress scale); $\sigma_1, \sigma_2, \sigma_3$ = observation-error standard deviations; B_S = observability-budget skill, the normalized CRPS reduction $(S_{\text{open}} - S_{\text{assim}})/(S_{\text{open}} - S_{\text{oracle}})$; T_C = water temperature, literature-informed model (deg C); $\tilde{g}(v)$ = normalized vegetation-contact factor; θ = Arrhenius coefficient.

References

Ahilan, S., M. Guan, N. Wright, A. Sleigh, D. Allen, S. Arthur, H. Haynes, and V. Krivtsov. 2019. "Modelling the long-term suspended sedimentological effects on stormwater pond performance in an urban catchment." *Journal of Hydrology*, 571: 805–818. https://doi.org/10.1016/j.jhydrol.2019.02.002.

Arnold, C. P., and C. H. Dey. 1986. "Observing-Systems Simulation Experiments: Past, Present, and Future." *Bulletin of the American Meteorological Society*, 67 (6): 687–695. https://doi.org/10.1175/1520-0477(1986)067%3C0687:OSSEPP%3E2.0.CO;2.

Bachand, P. A. M., and A. J. Horne. 1999. "Denitrification in constructed free-water surface wetlands: II. Effects of vegetation and temperature." *Ecological Engineering*, 14 (1-2): 17–32. https://doi.org/10.1016/S0925-8574(99)00017-8.

Barrett, M. E. 2005. "Performance Comparison of Structural Stormwater Best Management Practices." *Water Environment Research*, 77 (1): 78–86. https://doi.org/10.2175/106143005X41654.

Bellman, R., and K. J. Åström. 1970. "On structural identifiability." *Mathematical Biosciences*, 7 (3-4): 329–339. https://doi.org/10.1016/0025-5564(70)90132-X.

Commonwealth of Virginia. 2024. "9VAC25-900-110. Credit calculation procedures." Virginia Administrative Code, Title 9, Agency 25, Chapter 900.

Drake, J., and Y. Guo. 2008. "Maintenance of Wet Stormwater Ponds in Ontario." *Canadian Water Resources Journal*, 33 (4): 351–368. https://doi.org/10.4296/cwrj3304351.

Drusch, M., U. Del Bello, S. Carlier, O. Colin, V. Fernandez, F. Gascon, B. Hoersch, C. Isola, P. Laberinti, P. Martimort, A. Meygret, F. Spoto, O. Sy, F. Marchese, and P. Bargellini. 2012. "Sentinel-2: ESA's Optical High-Resolution Mission for GMES Operational Services." *Remote Sensing of Environment*, 120: 25–36. https://doi.org/10.1016/j.rse.2011.11.026.

Erickson, A. J., J. S. Gulliver, J.-H. Kang, P. T. Weiss, and C. B. Wilson. 2010. "Maintenance for Stormwater Treatment Practices." *Journal of Contemporary Water Research & Education*, 146 (1): 75–82. https://doi.org/10.1111/j.1936-704X.2010.00393.x.

Erickson, A. J., V. J. Taguchi, and J. S. Gulliver. 2018. "The Challenge of Maintaining Stormwater Control Measures: A Synthesis of Recent Research and Practitioner Experience." *Sustainability*, 10 (10): 3666. https://doi.org/10.3390/su10103666.

Evensen, G. 2003. "The Ensemble Kalman Filter: Theoretical formulation and practical implementation." *Ocean Dynamics*, 53 (4): 343–367. https://doi.org/10.1007/s10236-003-0036-9.

Gilliom, R. L., C. D. Bell, T. S. Hogue, and J. E. McCray. 2020. "Adequacy of Linear Models for Estimating Stormwater Best Management Practice Treatment Performance." *Journal of Sustainable Water in the Built Environment*, 6 (4): 04020016. https://doi.org/10.1061/JSWBAY.0000921.

Glasserman, P. 2004. *Monte Carlo Methods in Financial Engineering*. New York: Springer.

Gneiting, T., and A. E. Raftery. 2007. "Strictly Proper Scoring Rules, Prediction, and Estimation." *Journal of the American Statistical Association*, 102 (477): 359–378. https://doi.org/10.1198/016214506000001437.

Gold, A. C., S. P. Thompson, and M. F. Piehler. 2017. "Coastal stormwater wet pond sediment nitrogen dynamics." *Science of The Total Environment*, 609: 672–681. https://doi.org/10.1016/j.scitotenv.2017.07.213.

Hersbach, H. 2000. "Decomposition of the Continuous Ranked Probability Score for Ensemble Prediction Systems." *Weather and Forecasting*, 15 (5): 559–570. https://doi.org/10.1175/1520-0434(2000)015%3C0559:DOTCRP%3E2.0.CO;2.

Hoss, F., J. Fischbach, and E. Molina-Perez. 2016. "Effectiveness of Best Management Practices for Stormwater Treatment as a Function of Runoff Volume." *Journal of Water Resources Planning and Management*, 142 (11): 05016009. https://doi.org/10.1061/(ASCE)WR.1943-5452.0000684.

Huang, C., Y. Chen, S. Zhang, and J. Wu. 2018. "Detecting, Extracting, and Monitoring Surface Water From Space Using Optical Sensors: A Review." *Reviews of Geophysics*, 56 (2): 333–360. https://doi.org/10.1029/2018RG000598.

Kadlec, R. H. 2012. "Constructed marshes for nitrate removal." *Critical Reviews in Environ-*

mental Science and Technology, 42 (9): 934–1005. https://doi.org/10.1080/10643389.2010.534711.

Kadlec, R. H., and S. D. Wallace. 2009. *Treatment Wetlands*. 2nd ed. Boca Raton, FL: CRC Press.

Koch, B. J., C. M. Febria, M. Gevrey, L. A. Wainger, and M. A. Palmer. 2014. "Nitrogen Removal by Stormwater Management Structures: A Data Synthesis." *JAWRA Journal of the American Water Resources Association*, 50 (6): 1594–1607. https://doi.org/10.1111/jawr.12223.

Kumar, S. 2026. "A satellite-monitoring research agenda for urban stormwater infrastructure: Capabilities, gaps, and a community-benchmark proposal." EarthArXiv.

Lenhart, H. A., and W. F. Hunt. 2011. "Evaluating Four Storm-Water Performance Metrics with a North Carolina Coastal Plain Storm-Water Wetland." *Journal of Environmental Engineering*, 137 (2): 155–162. https://doi.org/10.1061/(ASCE)EE.1943-7870.0000307.

Li, J., R. R. Carlson, D. E. Knapp, and G. P. Asner. 2022. "Shallow coastal water turbidity monitoring using Planet Dove satellites." *Remote Sensing in Ecology and Conservation*, 8 (4): 521–535. Edited by K. Scales and A. Jones. https://doi.org/10.1002/rse2.259.

Liu, D., X. Zhu, M. Holgerson, S. Bansal, and X. Xu. 2024. "Inventorying ponds through novel size-adaptive object mapping using Sentinel-1/2 time series." *Remote Sensing of Environment*, 315: 114484. https://doi.org/10.1016/j.rse.2024.114484.

Liu, Y., B. A. Engel, D. C. Flanagan, M. W. Gitau, S. K. McMillan, I. Chaubey, and S. Singh. 2018. "Modeling framework for representing long-term effectiveness of best management practices in addressing hydrology and water quality problems: Framework development and demonstration using a Bayesian method." *Journal of Hydrology*, 560: 530–545. https://doi.org/10.1016/j.jhydrol.2018.03.053.

Lu, S., H. Hu, Y. Sun, and J. Yang. 2009. "Effect of carbon source on the denitrification in constructed wetlands." *Journal of Environmental Sciences*, 21 (8): 1036–1043. https://doi.org/10.1016/S1001-0742(08)62379-7.

Merriman, L., J. Hathaway, M. Burchell, and W. Hunt. 2017. "Adapting the Relaxed Tanks-in-Series Model for Stormwater Wetland Water Quality Performance." *Water*, 9 (9): 691. https://doi.org/10.3390/w9090691.

Min, J.-H., and W. R. Wise. 2009. "Simulating short-circuiting flow in a constructed wetland: The implications of bathymetry and vegetation effects." *Hydrological Processes*, 23 (6): 830–841. https://doi.org/10.1002/hyp.7219.

Moradkhani, H., S. Sorooshian, H. V. Gupta, and P. R. Houser. 2005. "Dual state–parameter estimation of hydrological models using ensemble Kalman filter." *Advances in Water Resources*, 28 (2): 135–147. https://doi.org/10.1016/j.advwatres.2004.09.002.

Nepf, H. M. 2012. "Flow and Transport in Regions with Aquatic Vegetation." *Annual Review of Fluid Mechanics*, 44 (1): 123–142. https://doi.org/10.1146/annurev-fluid-120710-101048.

Pekel, J.-F., A. Cottam, N. Gorelick, and A. S. Belward. 2016. "High-resolution mapping of global surface water and its long-term changes." *Nature*, 540 (7633): 418–422. https://doi.org/10.1038/nature20584.

Persson, J, Somes, N, and Wong, T. 1999. "Hydraulics efficiency of constructed wetlands and ponds." *Water Science and Technology*, 40 (3): 291–300. https://doi.org/10.1016/S0273-1223(99)00448-5.

Reichle, R. H. 2008. "Data assimilation methods in the Earth sciences." *Advances in Water Resources*, 31 (11): 1411–1418. https://doi.org/10.1016/j.advwatres.2008.01.001.

Sabokrouhiyeh, N., A. Bottacin-Busolin, M. Tregnaghi, H. Nepf, and A. Marion. 2020. "Variation in contaminant removal efficiency in free-water surface wetlands with heterogeneous vegetation density." *Ecological Engineering*, 143: 105662. https://doi.org/10.1016/j.ecoleng.2019.105662.

Taguchi, V. J., T. A. Olsen, P. Natarajan, B. D. Janke, J. S. Gulliver, J. C. Finlay, and H. G.

Stefan. 2020. “Internal loading in stormwater ponds as a phosphorus source to downstream waters.” *Limnology and Oceanography Letters*, 5 (4): 322–330. https://doi.org/10.1002/lol2.10155.

Tucker, C. J. 1979. “Red and photographic infrared linear combinations for monitoring vegetation.” *Remote Sensing of Environment*, 8 (2): 127–150. https://doi.org/10.1016/0034-4257(79)90013-0.

U.S. Environmental Protection Agency. 2026. “Three keys to BMP performance: Concentration, volume, and total load.” National Pollutant Discharge Elimination System.

U.S. Environmental Protection Agency, and Chesapeake Bay Program. 2003. *Storm water best management practice categories and pollutant removal efficiencies*. Annapolis, Maryland: U.S. Environmental Protection Agency, Chesapeake Bay Program Office.

Walter, E., and L. Pronzato. 1997. *Identification of Parametric Models from Experimental Data*. London: Springer.

Werner, T. M., and R. H. Kadlec. 2000. “Wetland residence time distribution modeling.” *Ecological Engineering*, 15 (1-2): 77–90. https://doi.org/10.1016/S0925-8574(99)00036-1.

Yang, Y., D. Z. Zhu, M. R. Loewen, S. S. Ahmed, W. Zhang, H. Yan, B. Van Duin, and K. Mahmood. 2023. “Evaluation of pollutant removal efficiency of urban stormwater wet ponds and the application of machine learning algorithms.” *Science of The Total Environment*, 905: 167119. https://doi.org/10.1016/j.scitotenv.2023.167119.